Stanford Exploration Project, Report 129, May 6, 2007, pages 19–33

Prestack depth migration in elliptic coordinates

Jeff Shragge and Guojian Shan

ABSTRACT

We extend Riemannian wavefield extrapolation (RWE) to prestack migration using 2D elliptic coordinate systems. The corresponding 2D elliptic extrapolation wavenumber introduces only a slowness model stretch to the single-square-root operator, enabling the use of existing Cartesian implicit finite-difference extrapolators for propagating wavefields. A zero-offset migration example illustrates the advantages of elliptic coordinates in imaging overturning wavefields. Imaging tests of the SMAART JV Pluto 1.5 and BP velocity benchmark data sets illustrate that the RWE migration algorithm generates high-quality prestack migration images equal to, or better than, the corresponding Cartesian coordinate systems. We still require higher-order extrapolators for accurate propagation and imaging using one-way wave equations, even in situations where RWE geometries are employed.

INTRODUCTION

Wave-equation migration techniques based on one-way extrapolators are often used to accurately image structure in complex geologic environments. Most conventional downward continuation approaches, though, are unable to handle the steeply propagating or overturning wavefield components often important for imaging areas of interest. A number of novel imaging approaches address these issues through a judicious decomposition of recorded wavefields (e.g. plane-wave migration (Whitmore, 1995)), partial or complete propagation domain decomposition (e.g. Gaussian beam (Hill, 2001) or Riemannian wavefield extrapolation (Sava and Fomel, 2005), respectively), or a combination thereof (e.g. plane-wave migration in tilted coordinates (Shan and Biondi, 2004)). Importantly, these techniques have overcome many, though not all, issues in the practical application of one-way extrapolation operators.

Riemannian wavefield extrapolation is a method for propagating wavefields on generalized coordinate meshes. The central idea behind RWE is transforming the geometry of the full domain to one where the extrapolation axis is oriented in the general wavefield propagation direction. Solving the corresponding one-way extrapolation equations propagates the bulk of wavefield energy at angles relatively close to the extrapolation axis, thus improving wavefield extrapolation accuracy. One obvious application is generating high-quality Green's functions for point-sources, where a ray-based coordinate system is first generated by ray-tracing through the velocity model and then used as the skeleton on which to propagate wavefields.

Although the full-domain decomposition approach naturally adapts to propagation in a point-source ray-coordinate system, two unresolved issues make it difficult to apply RWE

efficiently in the prestack domain. First, receiver wavefields are usually broadband in plane-wave dip spectrum and cannot be easily represented by a single coordinate system (i.e. opposing dips propagate in opposing directions). Second, optimal source and receiver meshes usually do not share a common geometry. This factor is detrimental to algorithmic efficiency where generating images by correlating source and receiver wavefields: by existing on different grids they must both be interpolated to a common Cartesian reference frame prior to imaging. This leads to a significant number of interpolations that leaves the algorithm computationally unattractive.

The main goal of this paper is to specify a single coordinate system that enables the accurate propagation of high-angle and overturning components of both the source and receiver wavefields. To these ends, we demonstrate that an elliptic coordinate system is a "natural" prestack shot-profile migration coordinate system exhibiting nice geometric properties. An elliptic coordinate system originates on the surficial plane and steps outward as a series of ellipses. Thus, the coordinate system expands in a radial-like manner appropriate for computing accurate point-source Green's functions, while allowing the receiver wavefield to propagate at steep (and overturning) angles to either side of the acquisition array where required. One consequence of using a 2D elliptic coordinate system is that the corresponding extrapolation wavenumber is specified by only a slowness model stretch. Thus, high-order implicit finite-difference (FD) extrapolators with accuracy up to 80° from the extrapolation axis (Lee and Suh, 1985) can be used to propagate wavefields, readily enabling accurate imaging of overturning waves at a cost competitive with Cartesian downward continuation.

This paper begins with a discussion as to why elliptic meshes are a natural coordinate system choice for shot-profile PSDM. We then develop an extrapolation wavenumber appropriate for propagating wavefields on 2D elliptic coordinate systems. We present a zero-offset example illustrating the ability of the scheme to image overturning wavefields. We then present prestack migration examples for the SMAART JV Pluto 1.5 and BP velocity benchmark data set and conclude with a brief discussion on the advantage of elliptic over more dynamic coordinate systems. Finally, Appendix A presents the wavenumbers for two 3D elliptic coordinates systems.

WHY ELLIPTIC COORDINATES?

Generating a good coordinate system for RWE prestack migration requires appropriately linking mesh geometry with the dynamics of propagating wavefields. Figure 1 illustrates this for an idealized shot-profile imaging experiment where source and receiver wavefields (S and R) are point sources defined at $[\mathbf{s}, \tau_s = 0]$ and $[\mathbf{r}, \tau_r = \tau]$ in a constant velocity medium $v(\mathbf{x})$. In this experimental setup, the wavefields expand outward as spherical wavefronts (dashed lines) described by

$$S(\mathbf{s},\mathbf{x};t) = \delta\left(t - \frac{||\mathbf{x}-\mathbf{s}||}{v(\mathbf{x})}\right) \quad \text{and} \quad R(\mathbf{r},\mathbf{x};t) = \delta\left(t - \tau - \frac{||\mathbf{x}-\mathbf{r}||}{v(\mathbf{x})}\right). \tag{1}$$

An image is generated by applying a correlation imaging condition at $t = 0$,

$$I(\mathbf{x}) = \sum_s \sum_r \delta \left[\tau - \left(\frac{||\mathbf{x}-\mathbf{r}|| + ||\mathbf{x}-\mathbf{s}||}{v} \right) \right], \tag{2}$$

which is the equation of ellipse (solid line). This suggests a natural link between elliptic coordinate systems and prestack migration, which is illustrated in Figure 1 by the similarity of the drawn isochron and the coordinate mesh.

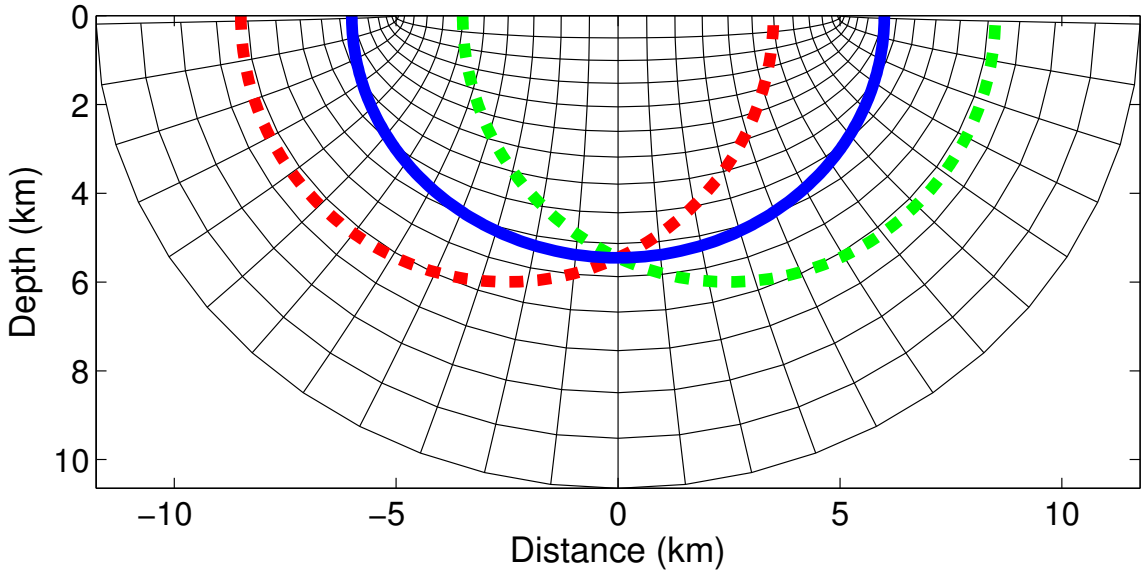

Figure 1: Idealized imaging experiment in a constant medium. Source and receiver wavefields (dashed lines) are expanding point sources described by fields $S(\mathbf{s},\mathbf{x};t)$ and $R(\mathbf{r},\mathbf{x};t)$. The corresponding image is an elliptic isochron surface $I(\mathbf{x})$ derived by cross-correlating the source and receiver wavefields (solid line). Note that the overlain elliptic coordinate system closely matches (though not identically) the isochron surface suggesting that this is a good coordinate system for RWE prestack shot-profile migration. jeff1-WhyEC [NR]

The keen observer will note that the foci of the elliptic coordinate system in Figure 1 were not specified relative to **s** and **r**. Shifting these points around alters both the mesh and how well it matches the isochrons. However, this represents two degrees of freedom that allow us to optimally match mesh geometry to the wavefield propagation dynamics.

ELLIPTIC COORDINATE EXTRAPOLATION

Propagating wavefields on elliptic meshes using RWE requires incorporating the geometry of the coordinate system directly in the extrapolation equations. This section derives the equations for propagation in the elliptic direction using the non-orthogonal RWE theory developed in Shragge (2006).

The analytic transformation between elliptic and Cartesian coordinate systems (see example in figure 1) is specified by,

$$\begin{bmatrix} x_1 \\ x_3 \end{bmatrix} = \begin{bmatrix} a\cosh\xi_3\cos\xi_1 \\ a\sinh\xi_3\sin\xi_1 \end{bmatrix}, \tag{3}$$

where $[x_1, x_3]$ are the underlying Cartesian coordinate variables, $[\xi_1, \xi_3]$ are the RWE elliptic coordinates, and a is a stretch parameter controlling the breadth of the coordinate system.

The metric tensor ($g_{ij} = \frac{\partial x_k}{\partial \xi_i}\frac{\partial x_k}{\partial \xi_j}$ with an implicit sum over index k) describing the geometry of the elliptic coordinate system is given by,

$$\left[g_{ij}\right] = \begin{bmatrix} A^2 & 0 \\ 0 & A^2 \end{bmatrix}, \tag{4}$$

where $A = a\sqrt{\sinh^2\xi_3 + \sin^2\xi_1}$. The determinant of the metric tensor is $|\mathbf{g}| = A^4$, leading to an associated (inverse) metric tensor given by,

$$\left[g^{ij}\right] = \begin{bmatrix} A^{-2} & 0 \\ 0 & A^{-2} \end{bmatrix}. \tag{5}$$

The weighted metric tensor (the product of the metric tensor and the determinant: $m^{ij} = \sqrt{|\mathbf{g}|}\, g^{ij}$) is given by,

$$\left[m^{ij}\right] = \begin{bmatrix} 1 & 0 \\ 0 & 1 \end{bmatrix}. \tag{6}$$

The corresponding extrapolation wavenumber is generated by using tensors g^{ij} and m^{ij} in the wavenumber expression for general 3D non-orthogonal coordinate systems (equations 13 and 14 in Shragge (2006)). Note that even though the elliptic coordinate system varies spatially, the local curvature parameters in the weighted metric tensor are constant. Thus, the extrapolation wavenumber, k_{ξ_3}, for recursive wavefield extrapolation stepping outward in concentric ellipses is,

$$k_{\xi_3} = \pm\sqrt{A^2 s^2\omega^2 - k_{\xi_1}^2}, \tag{7}$$

where $A = a\sqrt{\sinh^2\xi_3 + \sin^2\xi_1}$, s is slowness (inverse of velocity), and k_{ξ_1} is the orthogonal wavenumber. Equation 7 is an exact representation of the extrapolation wavenumber and does not contain any kinematic approximations. The most striking observation about this expression is that the sole difference between propagation in elliptic and Cartesian coordinate systems is a smooth multiplicative slowness model stretch. Otherwise, existing Cartesian extrapolators can be used for propagating wavefields.

2D SYNTHETIC TESTS

This section presents 2D test results for a zero-offset overturning wavefield and the prestack Pluto and BP velocity benchmark (Billette and Brandsberg-Dahl, 2005) data sets. We propagate all wavefields with the isotropic one-way extrapolator described in Lee and Suh (1985)

on a elliptic coordinate system defined by equation 3 assuming effective slowness fields of $A(\xi_1,\xi_3)s(\xi_1,\xi_3)$ where stretch factor A is defined above. We use generic zero-offset and shot profile migration algorithms employing the extrapolation wavenumber in equation 7 and then transform the results back to Cartesian using sinc-interpolation.

Poststack migration of overturning waves

The first elliptic coordinate migration example uses the zero-offset data set shown in the upper panel of Figure 2. The data were generated by Sava (2006) from an adapted Sigsbee model (lower panel) using exploding reflector (two-way time-domain FD) modeling from all salt body edges. Migrated multiples are present in the image below because we apply no multiple suppression prior to imaging. Note also that the time axis begins at 10 s and extends to 30 s. Figure 3 shows the migrated image obtained by wavefield extrapolation in elliptic coordinates.

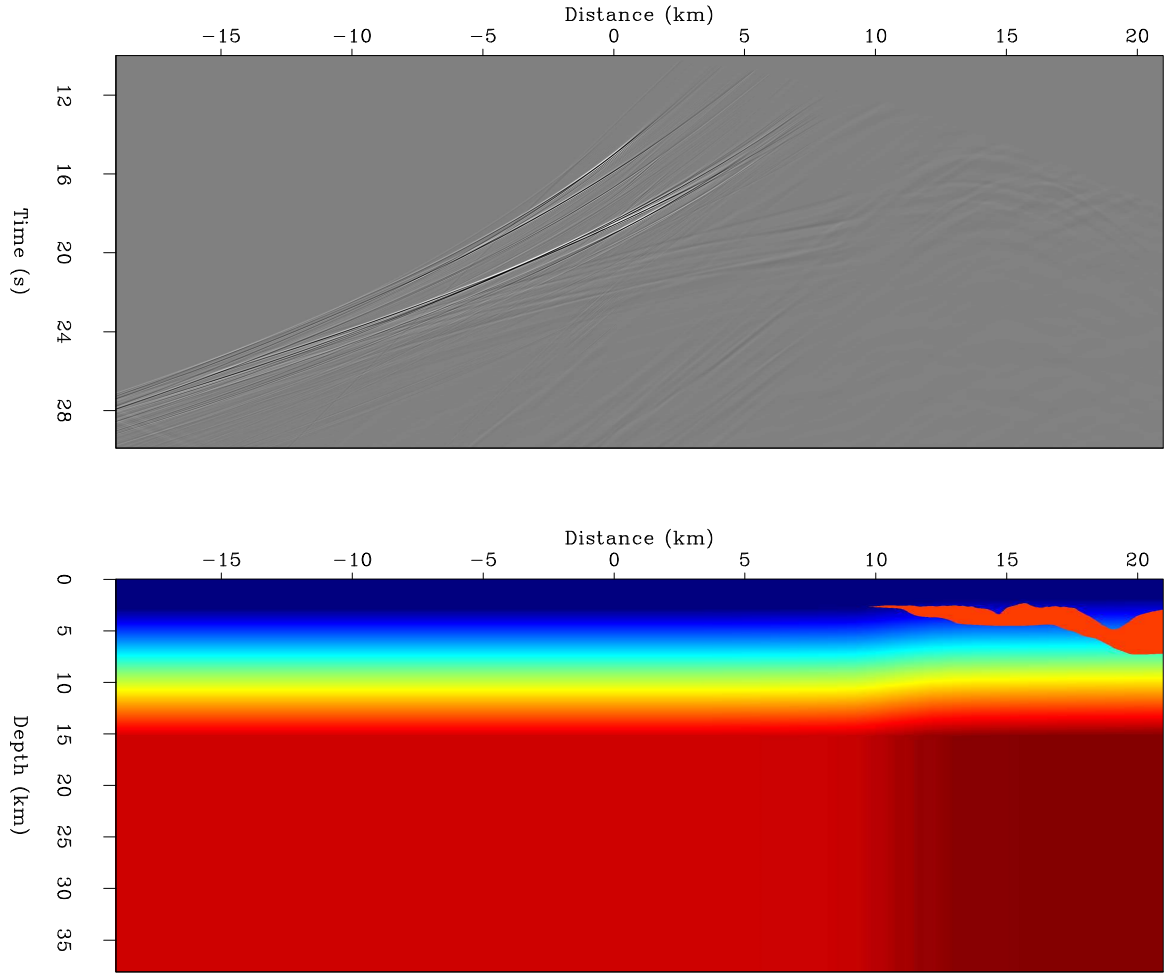

Figure 2: Overturning wavefield problem. Top: Exploding reflector data set generated through below model. Note that the time axis begins at 10s. Bottom: Migration velocity model. jeff1-OverProb [ER]

The upper left panel shows the prestack migration result for a monochromatic wavefield with the elliptic coordinate system overlain. The monochromatic wavefield overturns and arrives at the dipping salt flank at normal incidence, as expected for exploding reflector modeling. Note also that the wavefield energy propagates at fairly steep angles to the extrapolation axis indicating that high-angle accuracy extrapolators are necessary for accurate imaging. The upper right panel shows the same image as the upper left, but in the elliptic coordinate system. This figure similarly depicts the monochromatic wavefield propagating at high angle to the coordinate system. The lower left and right panels show the broadband image results in Cartesian and elliptic coordinate systems, respectively. The steep salt flanks beneath the salt nose are accurately positioned, indicating that the potential for imaging overturning waves in elliptic coordinates with high-angle accuracy propagators.

Prestack Pluto 1.5

Figure 4 presents a 2D prestack RWE migration test for the Pluto model. The top and middle panels show the elliptic coordinate and Cartesian migration results using 80° FD extrapolators. The bottom panel presents another Cartesian migration, but generated with lower-order phase-shift plus interpolation (PSPI) extrapolators. Note that the steeply dipping flanks on the left-most salt body are well-imaged in the upper two panels, but not as well in the lower panel. This suggests that higher-order extrapolators, rather than a new coordinate system, are needed to accurately image this salt flank. The image of the multiples beneath this salt body is more accurately migrated in the elliptic coordinate system, suggesting improved extrapolation has occurred in elliptic coordinates.

Prestack BP Velocity Model

We performed a second prestack migration test in elliptic coordinates using the BP velocity benchmark model. The top panel presents the RWE shot-profile migration result in elliptic coordinates, while the bottom panel shows Cartesian plane-wave image constructed with the same FD operators. The salt body on the left is well-imaged in both the elliptic and Cartesian coordinate images. The flanks of the salt body on the right, known to be illuminated by overturning and prismatic waves, are better imaged in the elliptic system. We generated the RWE image using a code that included neither source compensation nor optimal placement of the foci of the coordinate system. Furture work includes incorporating both of these factors, which should improve the image further.

Discussion

One question naturally arising when using RWE propagation in prestack migration is how does one obtain the optimal trade-off between: i) incorporating wave-propagation effects directly in a more dynamic coordinate system (e.g. through a ray-traced coordinate system); and ii) using higher-order extrapolators in coordinate systems not strictly conformal to the wavefield propa-

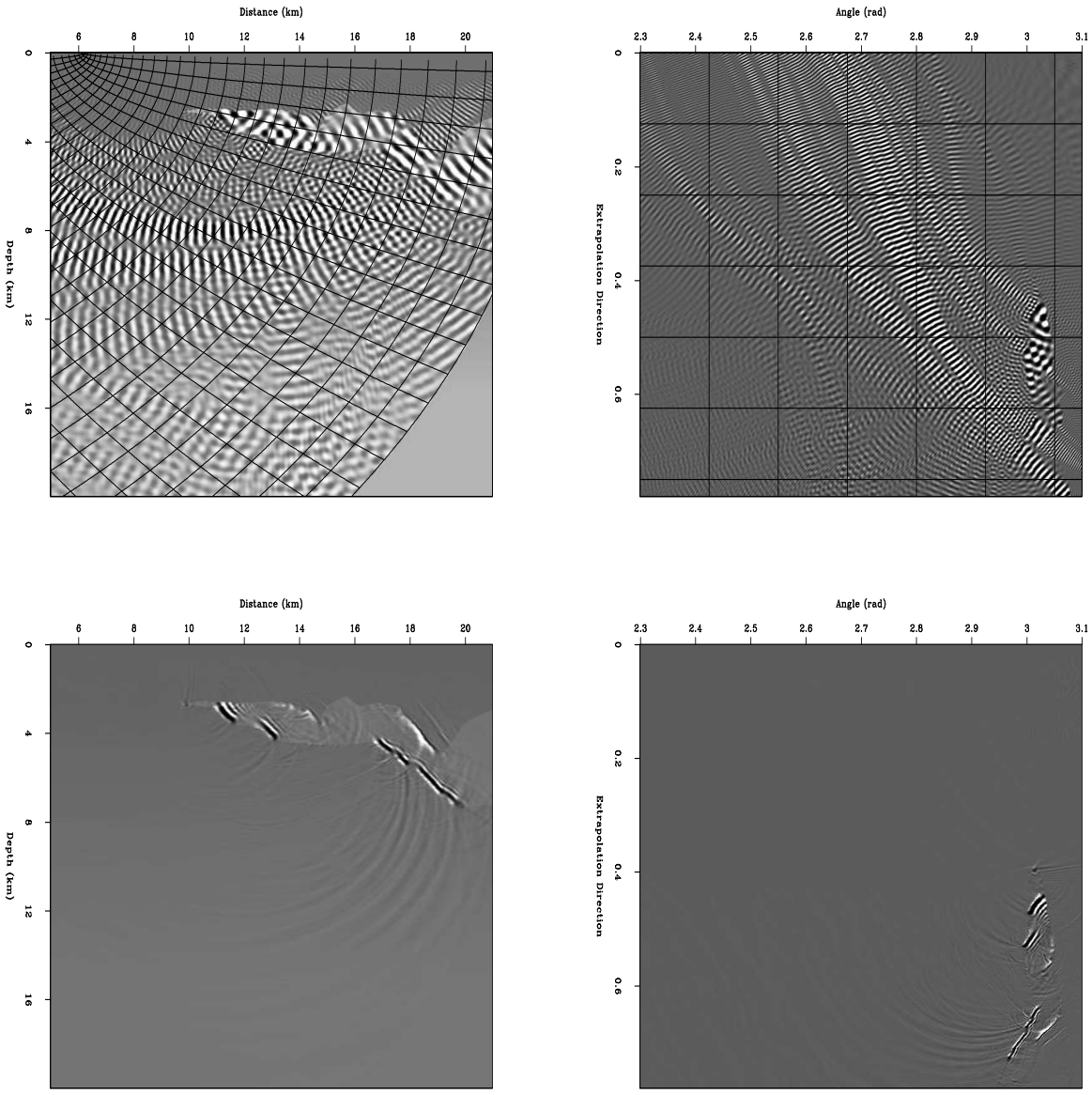

Figure 3: Post-stack migration of overturning waves. Upper left: Overturning monochromatic Cartesian wavefield with overlain elliptic coordinates. Top right: As in upper left panel, but for elliptic coordinates. Lower left: Broadband overturning wave image in Cartesian coordinates. Lower right: As in lower left panel, but for elliptic coordinates. jeff1-XM [CR]

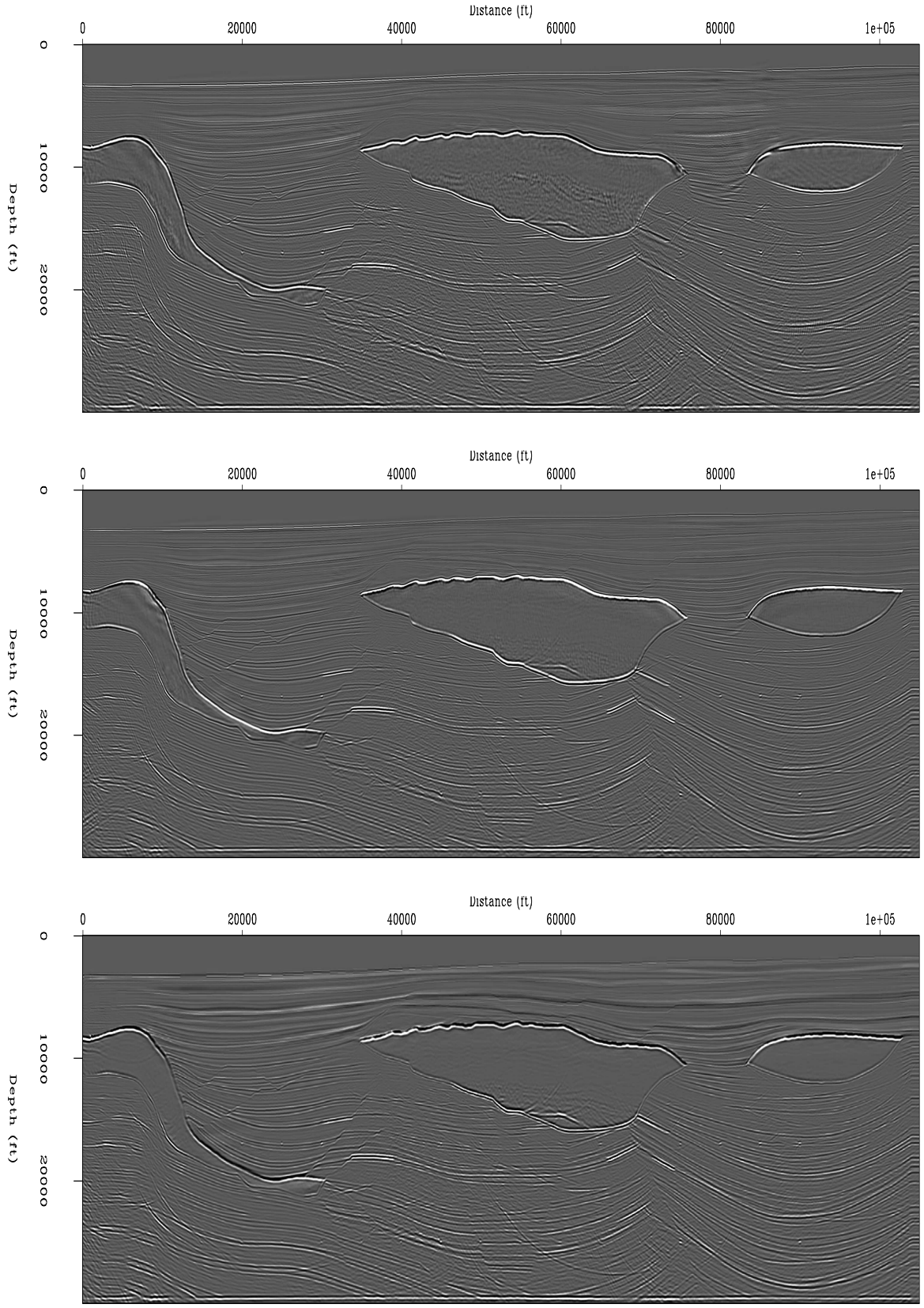

Figure 4: Pluto migration images for various coordinate systems and propagators. Top: Elliptic coordinates with FD propagators. Middle: Cartesian coordinates with FD propagators. Bottom: Cartesian coordinates with PSPI propagators. jeff1-PLUTO [CR]

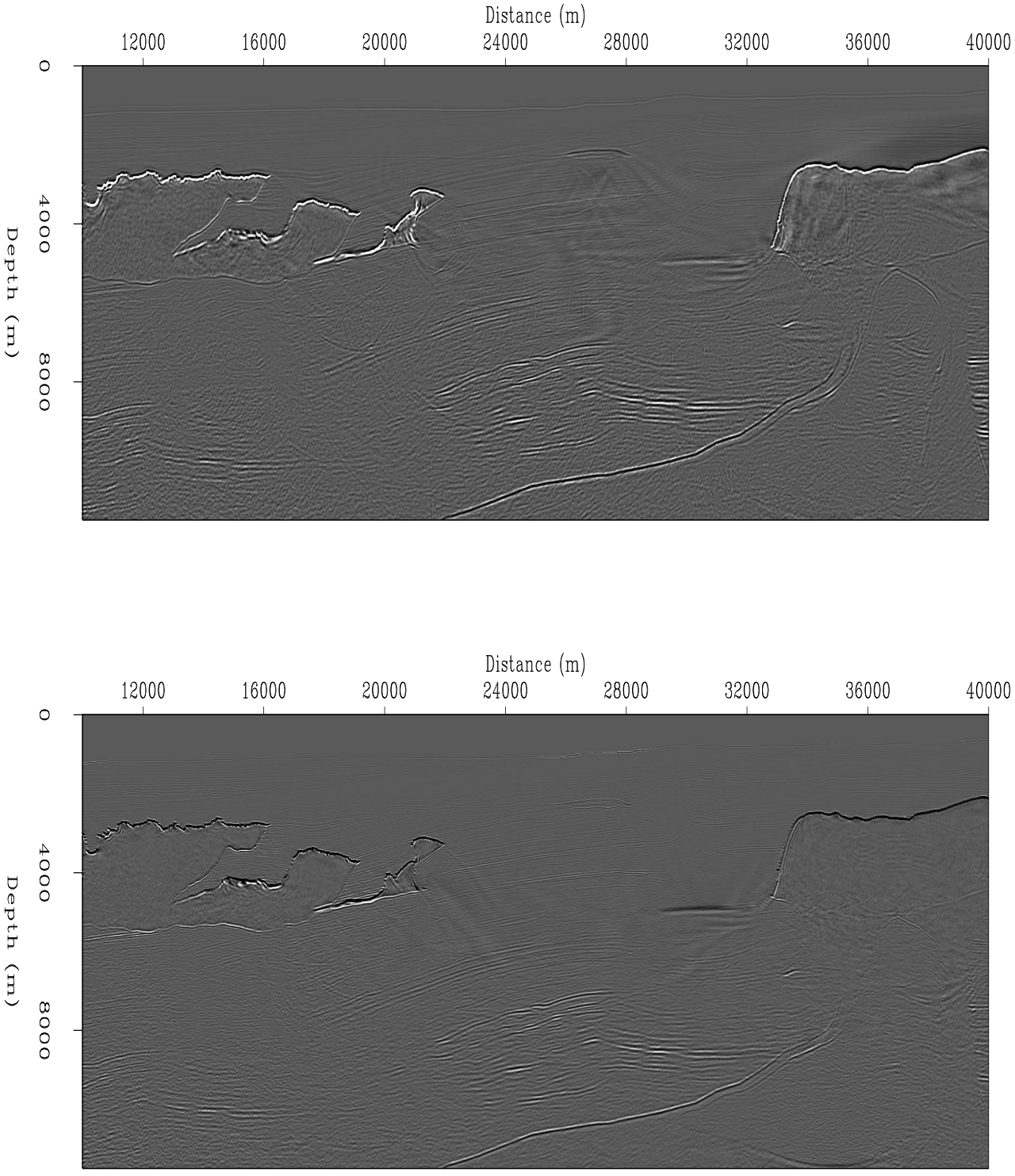

Figure 5: BP velocity synthetic migration results. Top panel: Elliptic coordinate migration result using FD propagators. Bottom panel: Cartesian migration result using FD propagators. jeff1-BPM [CR]

gation direction. Based on our experience, we argue that a parametric coordinate system (such as tilted Cartesian or elliptic meshes) offers the advantage of being able to develop analytic extrapolation operators that readily lend themselves to accurate, high-order, finite-difference schemes. Importantly, while coordinate systems based on ray-tracing better conform to the direction of wavefield extrapolation, numerically generated meshes do not lend themselves as easily to high-order extrapolators due to the greater number, and spatially variability of, the mixed-domain coefficients.

A second question worth addressing is how can the elliptic coordinate approach be extended to 3D prestack shot-profile migration. Appendix A presents two candidate coordinate systems. The elliptic cylindrical system extends the 2D elliptic by constant factor in the third dimension and realizes a fairly basic expression for the extrapolation wavenumber. This coordinate system, though, does not propagate overturning waves in the cross-line direction. The second coordinate system, oblate spheroidal, incorporates more spherical geometry and enables overturning wave propagation in the cross-line direction, but yields a more complicated extrapolation wavenumber. As expected, both of these coordinate systems reduce to the above 2D elliptic expression for a zero cross-line wavenumber.

CONCLUDING REMARKS

This paper extends the theory of Riemannian wavefield extrapolation to prestack shot-profile migration. An elliptic coordinate system is chosen because it generally conforms to the direction of propagation and allows high-angle propagation of source and receiver wavefields. Post-stack migration results of an overturning wavefield data set validate the approach, while the 2D prestack imaging results show that the RWE migration algorithm generates high-quality migration images equal to, or better than, the corresponding Cartesian domain. Finally, because one can develop analytic extrapolation wavenumbers, we argue that parametric coordinate systems are an optimal trade-off between the competing constraints of dynamic constraints and simplicity in coordinate system design.

ACKNOWLEDGMENTS

We thank Biondo Biondi, Ben Witten and Brad Artman for enlightening discussions. We thank the SEP sponsors for their continuing support. We acknowledge the SMAART JV consortium for the Pluto data and BP for the synthetic velocity data set.

REFERENCES

Billette, F. and S. Brandsberg-Dahl, 2005, The 2004 BP velocity benchmark: 67th meeting, Eur. Assn. Geosci. Eng., B035.

Hill, N. R., 2001, Prestack Gaussian-beam depth migration: Geophysics, **66**, 1240–1250.

Lee, M. W. and S. Y. Suh, 1985, Optimization of one-way wave-equations (short note): Geophysics, **50**, no. 10, 1634–1637.

Sava, P. C. and S. Fomel, 2005, Riemannian wavefield extrapolation: Geophysics, **70**, T45–T56.

Sava, P., 2006, Imaging overturning reflections by Riemannian Wavefield Extrapolation: Journal of Seismic Exploration, **15**, 209–223.

Shan, G. and B. Biondi, 2004, Imaging overturned waves by plane-wave migration in tilted coordinates: 74th Ann. Internat. Mtg., Soc. of Expl. Geophys., Expanded Abstracts, 969–972.

Shragge, J., 2006, Non-orthogonal Riemannian wavefield extrapolation: 75^{th} SEG Ann. Gen. Meeting and Exhibition, Expanded Abstracts, 2236–2240.

Whitmore, N. D., 1995, An imaging hierarchy for common angle plane wave seismograms: University of Tulsa, Ph.D. thesis.

APPENDIX A - 3D ELLIPTIC COORDINATE SYSTEMS

This appendix develops the dispersion relationship for extrapolating waves for two 3D elliptic coordinate systems: elliptic cylindrical and oblate spheroidal.

Elliptic Cylindrical Coordinates

The analytic transformation between the elliptic cylindrical and Cartesian coordinate systems (see example in figure A-1). A elliptical coordinate system is specified by,

$$\begin{bmatrix} x_1 \\ x_2 \\ x_3 \end{bmatrix} = \begin{bmatrix} a\cosh\xi_3\cos\xi_1 \\ \xi_2 \\ a\sinh\xi_3\sin\xi_1 \end{bmatrix}, \tag{A-1}$$

where $[x_1, x_2, x_3]$ are the underlying Cartesian coordinate variables, $[\xi_1, \xi_2, \xi_3]$ the RWE elliptic cylindrical coordinates, and parameter a a stretch parameter controlling the breadth of the coordinate system. The metric tensor describing the geometry of the elliptic coordinate system

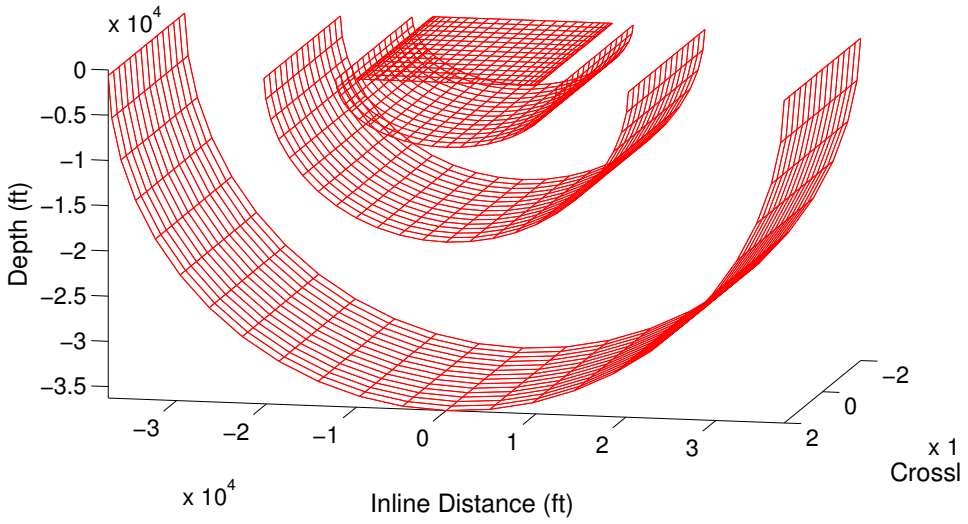

Figure A-1: Four sample extrapolation steps of an elliptic cylindrical coordinate system. jeff1-ECC [NR]

is given by,

$$\left[g_{ij}\right] = \begin{bmatrix} A^2 & 0 & 0 \\ 0 & 1 & 0 \\ 0 & 0 & A^2 \end{bmatrix}, \tag{A-2}$$

where $A = a\sqrt{\sinh^2\xi_3 + \sin^2\xi_1}$. The determinant of the metric tensor is: $|\mathbf{g}| = A^4$. The associated (inverse) metric tensor is given by,

$$\left[g^{ij}\right] = \begin{bmatrix} A^{-2} & 0 & 0 \\ 0 & 1 & 0 \\ 0 & 0 & A^{-2} \end{bmatrix}, \tag{A-3}$$

and weighted metric tensor ($m^{ij} = \sqrt{|\mathbf{g}|}\, g^{ij}$) is given by,

$$\left[m^{ij}\right] = \begin{bmatrix} 1 & 0 & 0 \\ 0 & A^2 & 0 \\ 0 & 0 & 1 \end{bmatrix}. \tag{A-4}$$

The corresponding extrapolation wavenumber is generated by using tensors g^{ij} and m^{ij} in the general wavenumber expression for 3D non-orthogonal coordinate system Shragge (2006). Note that even though the elliptic coordinate system varies spatially, the local curvature parameters remain constant: $n_1 = n_2 = n_3 = 0$. Thus, inserting the values of g^{ij}, m^{ij} and n_j leads to the following extrapolation wavenumber for stepping outward in concentric ellipses k_{ξ_3},

$$k_{\xi_3} = \pm\sqrt{A^2 s^2\omega^2 - k_{\xi_1}^2 - A k_{\xi_2}^2}. \tag{A-5}$$

The wavenumber for 2D extrapolation in elliptic coordinates reduces to

$$k_{\xi_3}\big|_{k_{\xi_2}=0} = \pm\sqrt{A^2 s^2\omega^2 - k_{\xi_1}^2}. \tag{A-6}$$

Note that equation A-5 does not contain a kinematic approximation of the extrapolation wavenumber.

Oblate Spheroidal Coordinates

The analytic transformation between the oblate spheroidal and Cartesian coordinate systems (see example in figure A-2). A elliptical coordinate system is specified by,

$$\begin{bmatrix} x_1 \\ x_2 \\ x_3 \end{bmatrix} = \begin{bmatrix} a\cosh\xi_3\cos\xi_1\cos\xi_2 \\ a\cosh\xi_3\cos\xi_1\sin\xi_2 \\ a\sinh\xi_3\sin\xi_1 \end{bmatrix}. \tag{A-7}$$

where, again, a is a stretch parameter controlling the breadth of the coordinate system. The metric tensor g_{ij} describing the geometry of oblate spheroidal coordinates is given by,

$$\left[g_{ij}\right] = \begin{bmatrix} A^2 & 0 & 0 \\ 0 & B^2 & 0 \\ 0 & 0 & A^2 \end{bmatrix}, \tag{A-8}$$

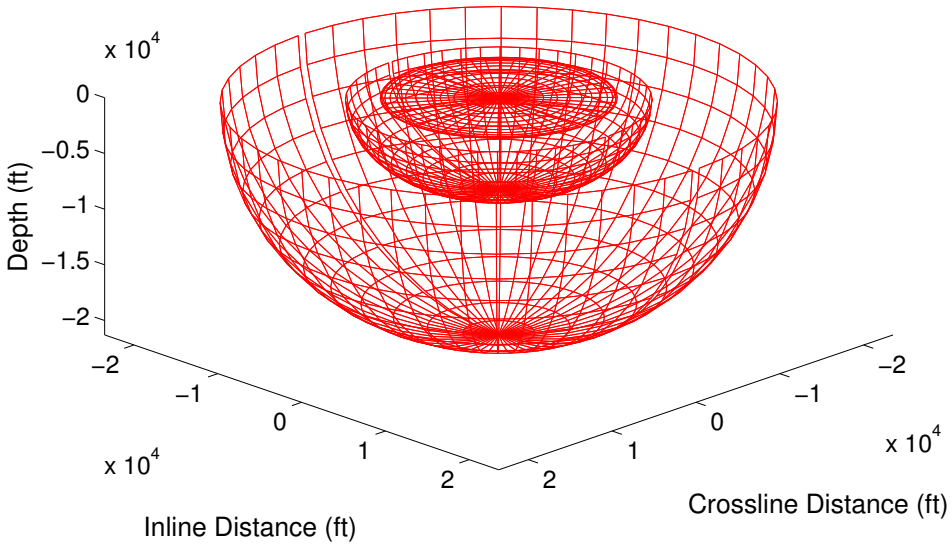

Figure A-2: Three sample extrapolation steps of an oblate spheroidal coordinate system. jeff1-OSC [NR]

where $A = a\sqrt{\sinh^2\xi_3 + \sin^2\xi_1}$ and $B = a\cosh\xi_3\cos\xi_1$. The determinant of the metric tensor is: $|\mathbf{g}| = A^4\,B^2$. The associated (inverse) metric tensor is given by,

$$\left[g^{ij}\right] = \begin{bmatrix} A^{-2} & 0 & 0 \\ 0 & B^{-2} & 0 \\ 0 & 0 & A^{-2} \end{bmatrix}. \tag{A-9}$$

and weighted metric tensor is given by,

$$\left[m^{ij}\right] = \begin{bmatrix} B & 0 & 0 \\ 0 & \frac{A^2}{B} & 0 \\ 0 & 0 & B \end{bmatrix}. \tag{A-10}$$

The corresponding extrapolation wavenumber is generated by inputting tensors g^{ij} and m^{ij} into the generalized wavenumber expression for 3D non-orthogonal coordinate systems (Shragge, 2006). Unlike in elliptic cylindrical coordinates, though, the oblate spheroidal system has non-stationary n^i coefficients: $n^1 = a\cosh\xi_3\sin\xi_1$, $n^2 = 0$ and $n^3 = a\sinh\xi$. The resulting extrapolation wavenumber is

$$k_{\xi_3} = \frac{\mathrm{i}\tanh\xi_3}{2} \pm \sqrt{A^2s^2\omega^2 - k_{\xi_1}^2 - \frac{\sqrt{\sinh^2\xi_3 + \sin^2\xi_1}}{\cosh\xi_3\cos\xi_1}k_{\xi_2}^2 + \mathrm{i}k_{\xi_1}\tan\xi_1 - \tanh^2\xi_3}. \tag{A-11}$$

The wavenumber for 2D extrapolation in elliptic coordinates reduces to

$$k_{\xi_3}\big|_{k_{\xi_2}=0} = \pm\sqrt{A^2s^2\omega^2 - k_{\xi_1}^2}. \tag{A-12}$$